

Schrödinger’s FP: Dynamic Adaptation of Floating-Point Containers for Deep Learning Training

Miloš Nikolić

University of Toronto

milos.nikolic@mail.utoronto.ca

Enrique Torres Sanchez

University of Toronto

enrique.torres@mail.utoronto.ca

Jiahui Wang

University of Toronto

eduardojh.wang@mail.utoronto.ca

Ali Hadi Zadeh

University of Toronto

hadizade@ece.utoronto.ca

Mostafa Mahmoud

University of Toronto

mostafa.mahmoud@mail.utoronto.ca

Ameer Abdelhadi

University of Toronto

ameer.abdelhadi@utoronto.ca

Andreas Moshovos

University of Toronto

moshovos@ece.utoronto.ca

Abstract—We introduce a software-hardware co-design approach to reduce memory traffic and footprint during training with BFloat16 or FP32 boosting energy efficiency and execution time performance. We introduce methods to dynamically adjust the size and format of the floating-point containers used to store activations and weights during training. The different value distributions lead us to different approaches for exponents and mantissas. *Gecko* exploits the favourable exponent distribution with a loss-less delta encoding approach to reduce the total exponent footprint by up to 58% in comparison to a 32 bit floating point baseline. To contend with the noisy mantissa distributions, we present two lossy methods to eliminate as many as possible least significant bits while not affecting accuracy. *Quantum Mantissa*, is a machine learning-first mantissa compression method that taps on training’s gradient descent algorithm to also learn minimal mantissa bitlengths on a per-layer granularity, and obtain up to 92% reduction in total mantissa footprint. Alternatively, *BitChop* observes changes in the loss function during training to adjust mantissa bit-length network-wide yielding a reduction of 81% in footprint. *Schrödinger’s FP* implements hardware encoders/decoders that guided by *Gecko/Quantum Mantissa* or *Gecko/BitChop* transparently encode/decode values when transferring to/from off-chip memory boosting energy efficiency and reducing execution time.

I. INTRODUCTION

Training most state-of-the-art neural networks has become an exascale class task [1], [2] requiring many graphics processors [3] or specialized accelerators such as the TPU [4], Gaudi [5], DaVinci [6], or Cerebras CS1 [7]. The need for energy efficient and fast inference further increases training costs as additional processing is needed during training to best tune the resulting neural network. Techniques such as quantization [8]–[11], pruning [12]–[14], network architecture search [15], and hyperparameter exploration [16] are examples of such training-time tuning techniques. The need for improving training speed and energy efficiency is not limited to server-class installations. Such methods are desirable also at the “edge” where training can be used to refine an existing model with user-specific information and input.

Improving training speed and energy efficiency has been receiving the attention it deserves throughout the software/hardware stack. Distributed training reduces training time by exploiting model, data, and pipeline parallelism [17], [18]. Dataflow optimizations such as data blocking and reuse, and communication and computation overlapping improve performance and energy efficiency by best allocating and using compute, memory and communication resources within and across computing nodes [19]–[21]. Transfer learning, can reduce training time and customization of a neural network by utilizing another previously training network as the basis upon which to train a refined model [22].

Regardless of whether training is done using a single node, or is distributed across several such as in federated [23] and distributed learning, single node performance and energy efficiency remains critically important. While training is both computationally and data demanding, it is memory transfers that dominate overall execution time and energy [24]. As reviewed in Section III, energy and time are dominated by data transfers for *stashing* (saving and much later recovering) activation and weight tensors [24]. Chen et al., have proposed recomputing activation tensors rather than stashing them [25] shifting the energy costs to compute rather than memory. Data blocking the form of micro-batching improves memory hierarchy utilization [26].

Another class of relevant solutions revisit the datatype used during training. Initially, training used single precision floating-point data and arithmetic as the focus was on demonstrating that neural networks can indeed tackle challenging problems. Since then, more compact datatypes such as half precision floating-point FP16, BFloat16 [27]–[29], dynamic floating-point [30], and flexpoint [31] have been introduced reducing overall traffic, and improving energy efficiency for computations and memory. Rather than using a single datatype throughout, which has to provide the precision needed by *all* data and computations, other methods explored using a combination of datatypes where more compact datatype are used for some if not most data and

computations [30], [32]–[34]. Finally, methods that use low bitlength arithmetic have also been proposed [35].

Complementing the aforementioned methods are lossless and lossy compression approaches that use fewer bits to represent stashed tensor content thus reducing overall traffic and footprints while improving energy efficiency and overall execution time [24], [36]–[38]. By boosting the effective capacity of each node’s memory compression techniques can also reduce inter-node traffic during distributed training. The methods target specific value patterns such as zeros, or take advantage of the underlying mathematical properties of training to use efficient representations of certain tensors (such as the outputs of ReLU or pool layers). Gist demonstrated that some models can be trained using tighter floating-point representations where the mantissa and exponent are using fewer bits compared to Bfloat16 or FP32 [24]. Gist does not offer a method for determining which representation to use in advance. The user has to try to train the network to determine whether it can still converge. Furthermore, Gist does not adjust the representation which remains the same throughout training.

This work explores *Schrödinger’s FP*, a family of lossy compression methods that complement prior aforementioned training acceleration methods. *Schrödinger’s FP* explores whether it is possible to *dynamically* and *continuously* adjust the *mantissa bitlength* (how many fractional bits) and the *container* (how many bits overall) for floating-point values for stashed tensors and to do so as much as possible *transparently* (without anyone looking). That is, *Schrödinger’s FP* is designed to work with existing training methods where it encodes values as they are being stashed to off-chip memory, and decodes them to their original format (we study FP32 and BFloat16) as they are being read back. As a result, *Schrödinger’s FP* can be used with any training hardware without requiring changes to the existing on-chip memory hierarchy and compute units.

Fundamentally, compression relies on non-uniformity in the data value distribution statically and temporally. It is instructive to compare and contrast the behavior of floating-point values during training with the fixed-point values commonly used during inference as many techniques have capitalized on the properties of the value stream during inference [36], [39]–[44]. During inference: 1) Zeros are very common especially in models using ReLU. 2) The distribution of weights and activations during inference tend to be heavily biased around a centroid (often zero), with very few values having a magnitude close to the extremes of the value range and many “medium magnitude” values being exceedingly rare. This results in many values having long bit prefixes of 0 or 1 making it profitable to adapt the container bitlength accordingly. 3) The weights are statically known and can be pre-encoded. 4) Activations tend to be used quickly after production and may not need to be stored to off-chip memory. 5) It is possible to trim some of the least significant bits which are “noisy” yet not useful [45] further skewing the value distribution.

In contrast to inference, adapting the container and bitlength of floating-point values during training has to content with the following challenges: 1) be it weights or activations, the

values are changing continuously, 2) the initial values are random, 3) floating-point values comprise a sign, exponent, and a normalized mantissa where a skewed value distribution does not necessarily translate into a skewed distribution at the bit-level, 4) training often does minute updates to larger values and any method has to accommodate those updates which cannot be discarded as noise, and 5) activation values have to be stashed over much longer periods of time (produced during the forward pass and consumed during the backward pass).

Since the values are continuously changing at runtime, a dynamic method is desirable. Promisingly, while the initial values are random, training relatively quickly modifies them resulting in overall distributions that are non-uniform thus giving compression an opportunity to be effective. However, a challenge remains as this non-uniformity is obstructed by the use of a normalized mantissa coupled with an exponent. Specifically, even though the values produced after a while resemble the non-uniform distributions seen during inference, the normalized mantissa lacks the 0 or 1 bit prefixes that are common in fixed-point. At the same time, a fixed-point representation lacks the range and potentially the bitlengths needed to support the wide range of updates that stochastic gradient descent performs. Finally, with carefully chosen dataflow most of the gradients can be produced and consumed on-chip.

To address the aforementioned challenges *Schrödinger’s FP* uses different approaches for the mantissa and exponent which we study with FP32 and BFloat16. *Schrödinger’s FP* dynamically adjusts mantissa bitlengths in order to store and read fewer bits per number in off-chip memory. This work explores two such mantissa bitlength adaptation methods. The first, *Quantum Mantissa* harnesses the training algorithm itself to learn, on-the-fly the mantissa bitlengths that is needed per tensor/layer and continuously adapts those bitlengths per batch. *Quantum Mantissa* introduces a single learning parameter per tensor/layer and a loss function that measures the effects of the current bitlength selection. Learning these bitlength parameters incurs a negligible overhead compared to the savings from the resulting reduction in off-chip traffic. The experiments with *Quantum Mantissa* show that: 1) it is capable to reduce the mantissa bitlengths considerably (for example, down to 4 to 1 bits depending on the layer and epoch with BFloat16), and 2) the reductions are achieved fairly soon in the training process and remain relatively stable till the end (e.g., after epoch 5). However, the bitlengths vary per layer/tensor and fluctuate throughout capturing benefits that wouldn’t be possible with a static choice of bitlengths.

Motivated by the success of *Quantum Mantissa*, we explore the second mantissa adjustment method, *BitChop*, which is a history-based, hardware-driven approach that requires no additional loss function and parameters. *BitChop* interfaces with the otherwise unmodified training system only in that it needs to be notified of per batch updates to the existing loss. Using an exponential moving average of these changes to the loss, to adjust mantissa bitlength for the whole network. As long as the network seems to be improving, *BitChop* will attempt to use a shorter mantissa, otherwise keep it the same or even

increase it. The method proves effective, albeit it achieves lower reductions in mantissa length compared to *Quantum Mantissa*. This is expected since: 1) *Quantum Mantissa* harnesses the existing training process to continuously learn what bitlengths to use, and 2) *Quantum Mantissa* adjusts bitlengths per layer whereas *BitChop* uses one bitlength for all layers.

For the exponents we corroborate past findings that most of the exponents during training exhibit a heavily biased distribution [46]. Accordingly, *Schrödinger’s FP* uses a value-based approach where it stores exponent using only as many bits as necessary to represent their magnitude plus sign. Metadata encode the number of bits used. To reduce the overhead of this metadata, *Schrödinger’s FP* encodes exponents in groups.

Section V presents efficient hardware compressors/decompressors that operate on groups of otherwise unmodified floating-point values be it FP32 or BFloat16. The compressors accept an external mantissa length signal and pack the group of values using the aforementioned compression methods for the mantissas and exponents. The decompressors expand such compressed blocks back to into the original floating-point format.

We study *Schrödinger’s FP* with ResNet18 [47] and MobileNet V3 [48] trained on ImageNet [49]. For clarity, we report detailed results with ResNet18 with BFloat16 throughout the paper, concluding with overall performance and energy efficiency measurements for all models.

We highlight the following experimental findings:

- *Schrödinger’s FP* compression techniques find the necessary mantissa and exponent bitlengths to reduce memory footprint without noticeable loss of accuracy: SFP_{QM} reduces ResNet18 down to 14.7% and MobileNet V3 Small to 23.7% and SFP_{BC} to 24.9% and 27.2%, respectively
- *Schrödinger’s FP* compressor/decompressor contributions exploit the reduced footprint to obtain $2.34\times$ and $2.12\times$ performance improvement for SFP_{QM} and SFP_{BC} , respectively
- Crucially, *Schrödinger’s FP* excels at squeezing out energy savings with on average, $5.17\times$ and $3.77\times$ better energy efficiency for SFP_{QM} and SFP_{BC} , respectively

II. RELATED WORK

Schrödinger’s FP will generally work in conjunction with methods that partition, distribute, and reschedule the training work. Accordingly, we limit attention to methods that reduce the container size or the datatype used during training.

Gist demonstrated that the bulk of the memory transfers during training is due to stashed activations [24]. Gist’s two main compression methods target two classes of activations: those between a ReLU and a Pooling layer, and those between a ReLU and a Convolutional layer. For the first class it shows that one bit is enough, whereas for the second it takes advantage of the sparsity caused by ReLU and avoids storing the resulting zeros. As a third method, Gist explores whether using a reduced length floating-point format — which is chosen in advance and kept the same throughout — still allows the network to

converge. It shows that *some* models can still converge and the bitlength needed varies across models. Gist determines this per model bitlengths *post-mortem*, that is only *after* performing a full training run. Regardless, this choice is useful when a network has to be routinely retrained. In contrast to Gist, *Schrödinger’s FP* discovers on-the-fly which representation to use and does so *continuously* throughout the training process adapting as needed. Moreover, for exponents it takes advantage of their skewed value distribution adapting the number of bits used to their actual values instead of using a one-size-fits-all.

Mixed-precision methods use a mix of fixed-point and floating-point operations and values [30], [34]. The methods still use pre-decided and fixed during the training process data formats. Furthermore, they require modifications to the training implementation to take advantage of this capability. *Schrödinger’s FP* does not modify the training implementation, adjusts the data type and containers continuously, and encodes exponents based on their content. Xiao et al., demonstrated that training some models is possible performing the bulk of computations over extremely narrow formats using 4b (forward) and 8b (backward) albeit at some reduction in accuracy (roughly 2% absolute for MobileNet V2/ImageNet) [50]. In principle, given *Schrödinger’s FP’s* dynamic and content-based approach, it should be possible to combine it with such training methods boosting overall benefits. However, further study is needed to determine whether this is possible and effective.

Sakr et al., present an analytical method for predicting the accumulation bitlengths needed per layer/block with the main goal of reducing computation costs at the floating-point units [51]. The method produces tight, yet fixed-size formats for the whole training process. *Schrödinger’s FP* is a dynamic approach that also takes advantage of value content for exponents and that does not modify the training implementation. Studying the interaction and potential synergy with such analytical methods is interesting future work.

III. THE TRAINING PROCESS

Our goal is to make training more efficient. Accordingly, we will first briefly cover how the training process unfolds and indicate where the most costly actions are. Furthermore, one of our methods involves modifying the training process and that discussion will learn on the information in this section.

A task of a neural network can be almost anything, from natural language processing, recommendation systems, to computer vision [52]. While many tasks are best solved with feed-forward networks, some perform better with feed-back connections. However, feed-back connections can be unraveled in time to produce feed-forward networks [52]. Consequently, we focus on feed-forward networks.

The goal of training a network is to determine the parameters that will best solve the given task. Without loss of generality, we will focus on image classification networks as they are simplest to explain, were the first ones drive the resurgence in interest in deep learning, and remain as the most common benchmark for hardware evaluation.

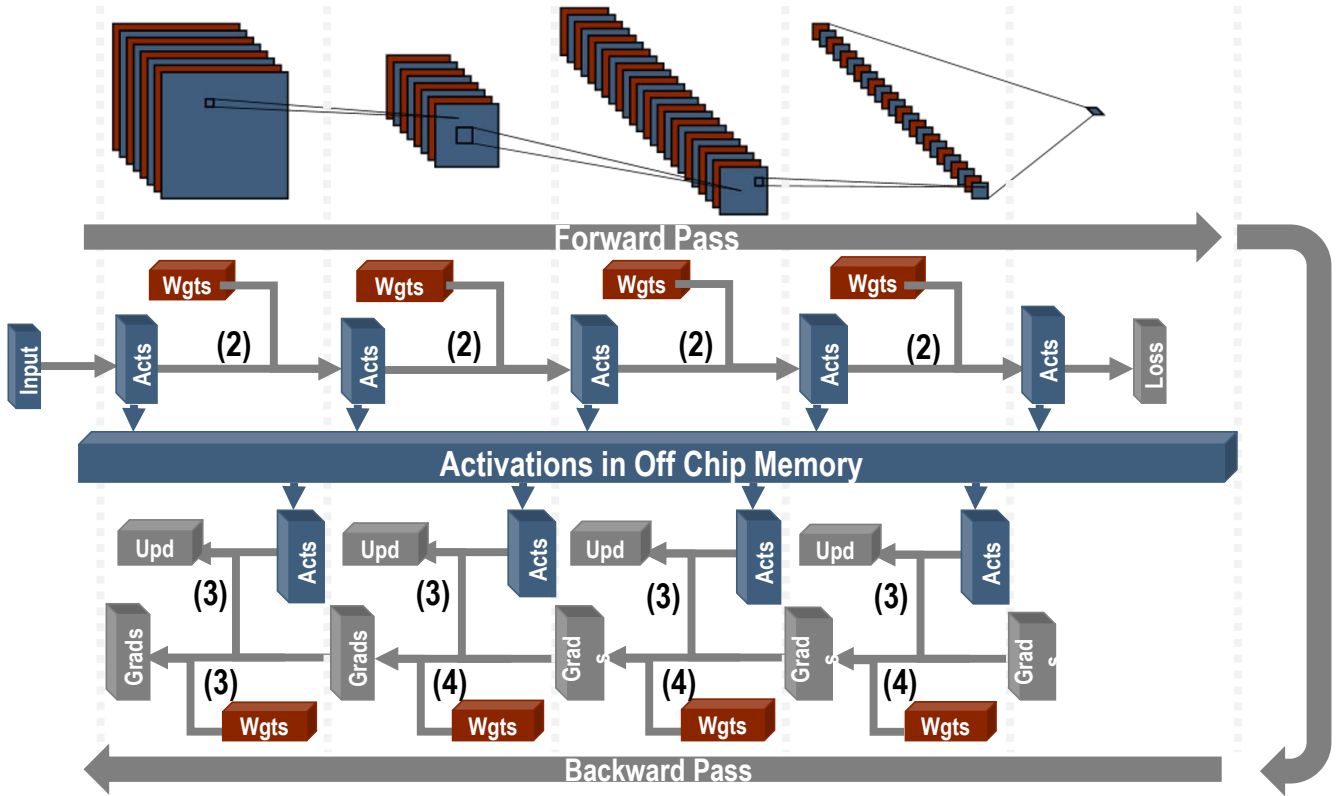


Fig. 1: Training process and its memory transfers. Numbers represent the equations that are computed. Blue - Activations that are typically saved to off-chip memory during forward pass and retrieved during backward pass, Red - Weights that are typically stored and loaded once from off-chip memory, Gray - Updates and Gradients – through mini-batching during the backward pass they can often fit on-chip.

In order to explain the training process, we will describe *Gradient Descent* by introducing the loss function in Section III-A, the forward pass in which we evaluate the performance of the network in Section III-B and the backward pass in which the parameters are updated in Section III-C. Finally, in Section III-D we will explain the scale of the problem. Figure 1 provides an overview of the training process illustrating tensor transfers.

A. The Loss Function

Training explicitly targets improving the value of a *Loss Function*. This is a function that acts as a proxy for the accuracy at solving the desired task. The requirements of this function is that it is differentiable and that the value of the function reduces as the output network approaches the desired value and the certainty of that output increases. In this case, the smaller the loss function, the more desirable the network performance.

If these conditions are satisfied, it is fairly simple to devise updates for all parameters. The partial derivative of the loss function in respect of each parameter indicates how a change of the parameter will affect the loss function. Since our goal is the minimize the loss function, we want to bump each parameter in the opposite direction of the partial derivative:

$$w_i^l = w_i^l - LR \times \frac{\delta L}{\delta w_i^l} \quad (1)$$

where w_i^l represents the i -th weight of layer l , LR represents the learning rate and L represents the Loss function.

We repeat this procedure for every parameter, for many inputs to slowly reach the weights at which the loss function is minimal, and as a result the accuracy is maximized. Crucially, if we want to optimize some property, say weight values, number of operations or memory footprint, we can include this in our Loss function and use the same procedure. In order to use this procedure to update the weight, every operation we use in the network must be differentiable.

B. Forward Pass

In the forward pass, we input the training example and calculate the Loss Function by sequentially calculating all the activations in order. This involves simply computing the output of each layer l sequentially:

$$a_i^{l+1} = F^l \left(\sum_j w_{i,j}^l \times a_{i,j}^l \right) \quad (2)$$

where a_i^{l+1} represents the i -th activation of layer $l+1$, $w_{i,j}^l$ and $a_{i,j}^l$ represent the weights and activations of layer l that are directly connected to a_i^{l+1} and F^l is a non-linear differentiable activation function of the l -th layer. The input activation of each layer, for every input, needs to be saved to in order to compute the backward pass.

C. Backward Pass

The backward pass utilizes the chain rule to progressively find the partial derivative of the loss function with respect to the weights. In this case, the reuse of calculated values is maximized. The process involves two steps for every layer, applied in reverse order, from the last to the first:

1) Weight Update: First we can compute the input the updated weights of the current layer:

$$w_i^l = w_i^l - LR \times \sum_j a_{i,j}^l \times \frac{\delta L}{\delta a_j^{l+1}} \quad (3)$$

where LR is the learning rate, $a_{i,j}^l$ are the activations connected to the weight and $\frac{\delta L}{\delta a_j^{l+1}}$ is the activation gradient from the $l+1$ -th layer.

2) Propagate Gradient Backward: Second, we propagate the gradient backward into the previous layer by computing:

$$\frac{\delta L}{\delta a_i^l} = \sum_j w_{i,j}^l \times \frac{\delta L}{\delta a_j^{l+1}} \times \frac{\delta F^l}{\delta a_j^l}(a_j^l) \quad (4)$$

where $w_{i,j}^l$ and $\times \frac{\delta L}{\delta a_j^{l+1}}$ are all weight/output gradient pairs connected to the input gradient and F^l is the activation function of layer l . Only at this point can the activations of this layer be discarded.

We repeat these steps all the way to the input layer. Once this is done we have completed one weight tensor update. We repeat this for every input batch, for many epochs.

D. So, why is training expensive?

While training is expensive both compute- and memory-wise, off-chip memory accesses dominate the energy and time costs [24] since computing the weight updates, necessitates retrieving the activations from the forward pass. This is a massive amount of data. For ImageNet, with reasonable batch sizes, the volume of activations is on the order of gigabytes far exceeding practical on-chip capacities.

E. Gradient Descent

The core of training remains the *Gradient Descent* procedure: slowly, step-by-step moving against the gradient to find the parameters that produce the minimum loss. This algorithm is being continuously improved to find better minima quicker and cheaper. However, the basics and hardware implications remain the same; lots of compute and even more memory.

F. Our Contribution

Our goal is to reduce the energy and time cost of training by leveraging machine learning and hardware techniques to reduce memory footprint and traffic. We do this by selecting an *elastic* datatype and container coupled with light-weight, custom encoder/decoder hardware that exploits it to reduce off-chip traffic and footprint. We propose:

1) two *lossy*, but controlled, techniques to reduce the number of mantissa bits. Since mantissas are normalized and almost uniformly distributed, our approach is to trim the mostly noisy, least significant bits with one of two, real-time novel techniques:

- *Quantum Mantissa:* A machine learning technique to find required mantissa bitlength introduced in Section IV-A. This technique involves a low-overhead modification of gradient descent to “learn” fine-grained (per tensor/layer) mantissa requirements during training.
- *BitChop:* A heuristic based technique that finds the activation mantissas in Section IV-B. This method tracks the current loss function and deciding whether to add, remove, or keep the same the activation mantissa bitlength at network-level granularity.

2) *Gecko:* A loss-less compression method for exponents by exploiting their favorable normal distribution (Section IV-C). This method relies on delta encoding and a fine-grained approach to significantly reduce the exponent footprint of both weights and activation.

3) A hardware architecture to exploit our custom datatype in Section V and deliver energy and performance benefits for neural network training.

IV. ADJUSTING VALUE CONTAINERS DURING TRAINING

The first step to reducing the energy and time cost of training is to define an efficient datatype. In general, training requires a floating-point approach in order to maintain accuracy on most real-world tasks. Floating-point formats consist of three distinct segments: a mantissa, an exponent, and a sign bit. Mantissas and exponents are differently distributed, so they require different approaches. The greatest challenge is compressing mantissas since they are uniformly distributed across the domain whereas compression exploits non-uniformity. We will present two approaches to compresses mantissas, an machine learning approach in Section IV-A and a hardware design inspired approach in Section IV-B. In contrast exponents can be compressed with fairly simple hardware techniques as shown in Section IV-C. We will briefly comment on the implications of the sign bit in Section IV-D. Finally, Section VI-A will bring it all together and show the full effects of our approach.

A. Mantissa: Quantum Mantissa

Quantum Mantissa involves procedures for both the forward and backward passes of training. We begin by defining a conventional quantization scheme for integer mantissa bitlengths in the forward pass and then expand it to the non-integer domain and then describe how this interpretation allows bitlengths to be learned using gradient descent. Subsequently, we introduce a parameterizable loss function, which enables

Quantum Mantissa to penalize larger bitlengths. We then briefly touch on the compute overhead of our method and the plan for final selection of mantissa bitlengths. Ultimately, we demonstrate the benefits of *Quantum Mantissa* on memory footprint during ImageNet training.

1) *Quantization*: The greatest challenge for learning bitlengths is that they represent discrete values over which there is no obvious differentiation. To overcome this challenge we define a quantization method on non-integer bitlengths. We start with an integer quantization of the mantissa M with n bits by zeroing out all but the top n bits:

$$Q(M, n) = M \wedge (2^n - 1) \ll (m - n) \quad (5)$$

where $Q(M, n)$ is the quantized mantissa with bitlength n , m is the maximum number of bits and \wedge represents bitwise AND.

Throughout training, we represent the integer quantization as $Q(M, n)$. This quantization scheme does not allow the learning of bitlengths with gradient descent due to its discontinuous and non-differentiable nature. To expand the definition to real-valued $n = \lfloor n \rfloor + \{n\}$, the values used in inference during training are selected as a random choice between the nearest two integers with probabilities $\{n\}$ and $1 - \{n\}$:

$$Q(M, n) = \begin{cases} Q(M, \lfloor n \rfloor), & \text{with probability } 1 - \{n\} \\ Q(M, \lfloor n \rfloor + 1), & \text{with probability } \{n\} \end{cases} \quad (6)$$

where $\lfloor n \rfloor$ and $\{n\}$ are floor and fractional parts of n , respectively. The scheme can be, and in this work is, applied to activations and weights separately. Since the minimum bitlength per value is 0, n is clipped at 0. This presents a reasonable extension of the meaning of bitlength in continuous space and allows for the loss to be differentiable with respect to bitlength.

During the forward pass the above formulae are applied to both activations and weights. The quantized values are saved and used in the backward pass. During the backward pass we use the straight-through estimator [53], [54] to prevent propagating zero gradients that result from the discontinuity’s discreteness, however, we use the quantized mantissas for all calculations. This efficient quantization during the forward pass reduces the footprint of the whole process.

2) *Loss Function*: On top of finding the optimal weights, the modified loss function penalizes mantissa bitlengths by adding a weighted average (with weights λ_i not be confused with the model’s weights) of the bits m_i required for mantissas of weights and activations. We define total loss L as:

$$L = L_l + \gamma \sum (\lambda_i \times n_i) \quad (7)$$

where L_l is the original loss function, γ is the regularization coefficient used for selecting how aggressive the quantization should be, λ_i is the weight corresponding to the importance of the i^{th} group of values (one per tensor), and n_i is the bitlength of the activations or weights in that tensor.

This loss function can be used to target any quantifiable criteria by a suitable selection of the λ_i parameters. Since our goal is to minimize the total footprint of a training run, we weight each layer’s tensors according to their footprint.

3) *Computational and Memory Overheads*: *Quantum Mantissa* adds minimal computational and memory overhead to the forward and backward passes. In the forward pass, random numbers need to be created at a chosen granularity to determine the quantized values. Ideally this would be done per value, however, our experiments show that per tensor/layer is sufficient and is a negligible cost.

To update the bitlength parameters in the backward pass, we need to compute their gradients. These are a function of the weight values and gradients, which will be calculated as part of regular backward pass. As a result, the extra calculations for each bitlength is on the order of $O(n)$, where n is the number of values quantized to that bitlength. This overhead is negligible in comparison to the total number of computations. In the case of our experiments, the overhead is less than 2% and 0.5% for MobileNet V3 and ResNet18, respectively.

On the memory side, the only extra parameters that need to be saved are the bitlengths, two floats per layer (bitlength for weights and activations), again negligible in comparison with the total footprint. All other values are consumed as they are produced without need for off-chip stashing.

4) *Bitlength Selection*: The above training method will produce non-integer bitlengths and requires stochastic inference (given a fractional bitlength we choose one of the surrounding integer bitlengths at random per tensor). We prefer the network not to have this requirement when deployed. For this reason, we *round up* the bitlengths and fix them for some training time to fine-tune the network to this state. While our experiments show that bitlengths converge quickly and final ones can be determined within a couple of epochs avoiding the small overhead for most of training, we aim to delay this action so that bitlengths have the ability to increase if needed during training. Our experiments show that this unnecessary for the models studied, however, the overhead is so small that we leave it on as a safety mechanism. We round up the bitlengths for the last 10 epochs to let the network regain any accuracy that might have been lost due to *Quantum Mantissa*. *Quantum Mantissa* still reduces traffic during these epochs.

Evaluation: BitLengths and Accuracy: We report measurements for per-layer weights and activations quantized separately using a loss function weighted to minimize total memory footprint. We train ResNet18 [55] on the ImageNet [49] dataset over 90 epochs, with 0.1 weight decay, setting the regularizer strength to 0.1, 0.01 and 0.001 respectively at epochs 0, 30, and 60.

The goal of *Quantum Mantissa* is to tap onto the learning algorithm to minimize the memory footprint whilst not introducing accuracy loss. It excels at this goal. Figure 2 shows that throughout training *Quantum Mantissa* introduces minimal changes in validation accuracy. In the end, the network converges to a solution within 0.4% of the FP32 baseline.

Figure 3 shows how *Quantum Mantissa* quickly (within a couple of epochs) reduces the required mantissas for activations and weights down to 1 – 2 bits on average. Throughout training, the total cumulative memory footprint is reduced to 7.8% and 25.5% of the FP32 and BFloat16 mantissa

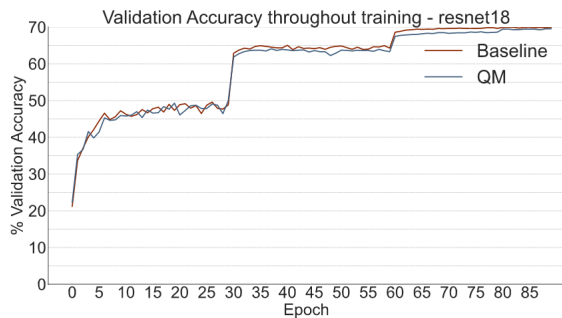


Fig. 2: *Quantum Mantissa*: ResNet18 validation accuracy throughout training

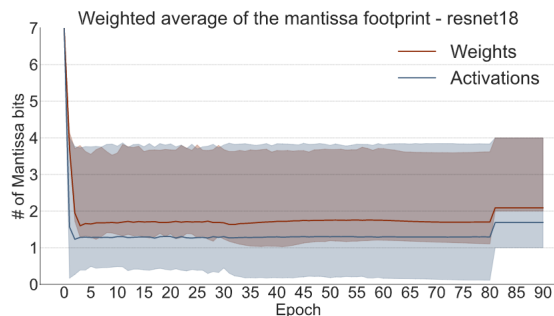


Fig. 3: *Quantum Mantissa*: ResNet18 weighted mantissa bitlengths with their spread throughout training

footprint, respectively. The figure further shows that there is a large spread across different layers, indicating that a granular, per-layer, approach is the right choice to maximize benefits. *Quantum Mantissa* generally targets the activation bitlengths more aggressively than the weights as the activations are responsible for the majority of the memory footprint. This is contrary to the case when the bitlengths are not weighted according to their importance and the weights end up being smaller than the activations.

The spread of mantissa bitlengths across the network and time is shown in Figure 4. While most layers quickly settle at 1 or 2 bits, there are a couple of exceptions that require more, at times up to 4b. Because of this spread, a network-scale datatype would have to use the largest datatype and leave a lot of the potential untapped. For ResNet18, the maximum bitlength is over $2\times$ larger than the weighted average.

B. Mantissa: *BitChop*

While *Quantum Mantissa* leverages training itself to greatly reduce mantissa lengths, having a method that does not require introducing an additional loss function and parameters would be appealing. *BitChop* is a run-time, heuristic method to reduce the number of mantissa bits for the forward and backward passes. At a high-level, *BitChop* monitors how training progresses adjusting the mantissa length accordingly: as long as the training seems to be improving the network, *BitChop* will attempt to use a shorter mantissa, otherwise it will try to

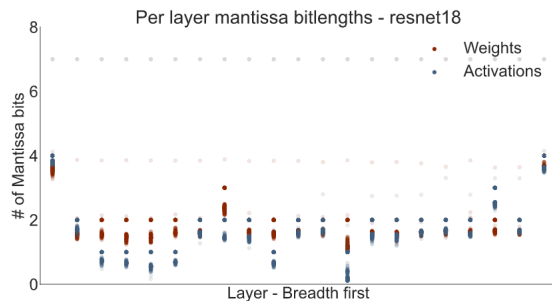


Fig. 4: *Quantum Mantissa*: Mantissa bitlengths for each layer of ResNet18 at the end of each epoch. Darker dots represent the latter epochs

increase its bitlength. Figure 5 illustrates *BitChop*'s “observe and adjust” approach. *BitChop* conceptually splits the training process into *periods*, where a period is defined as processing N batches. *BitChop* adjusts the mantissa at the end of each period using information about network progress.

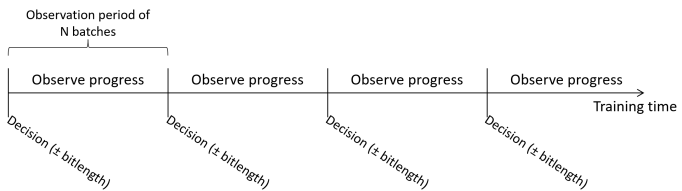


Fig. 5: *BitChop*'s Observe/Decide Approach

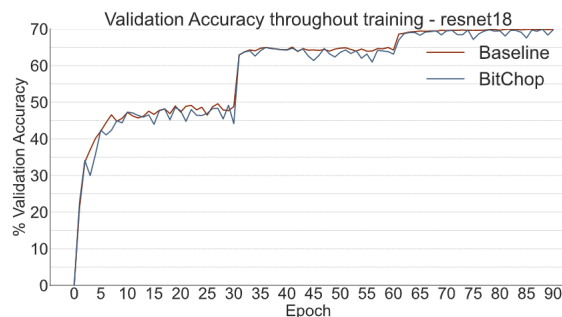


Fig. 6: *BitChop*: ResNet18/ImageNet validation accuracy throughout BFloat16 training

The ideal scenario for *BitChop* is one where past observation periods are good indicators of forthcoming behavior. Macroscopically, network accuracy improves over time during training, which appear to be a good fit. Microscopically, however, training is a fairly noisy process, a reality that *BitChop* has to content with. Fortunately, training is a relatively long process based on “trial-and-error” which may be forgiving for momentary lapses in judgement.

There are three major design decisions that impact how successful *BitChop* can be: 1) what information to use as a proxy for network progress, 2) how long the period should be, and 3) at what granularity to adjust mantissa lengths. The resulting method should strike a balance between capturing as

much as possible of the opportunity to reduce bitlength, while avoiding over-clipping as this can hurt learning progress and ultimately the final accuracy that will be achieved.

We have experimented with several options and arrived at the following choices: 1) Using an exponential moving average of the loss as a proxy for network progress, and 2) using a short period where $N = 1$, that is a single batch. Moreover, rather than attempting to adjust mantissas at the tensor/layer level, *BitChop* uses the same mantissa for the whole model.

In more detail, to monitor network progress, *BitChop* uses the loss which is calculated per batch as part of the regular training process. While the loss improves over time, when observed over short periods of time, it exhibits non-monotonic behavior which is sometimes erratic. To compensate for this volatility, *BitChop* uses an exponential moving average *Mavg* which it updates at the end of each period:

$$Mavg = Mavg + \alpha * (L_i - Mavg) \quad (8)$$

where L_i is the loss during the last period and α is an exponential decay factor which can be adjusted to assign more or less significance to older loss values. This smooths the loss over time while giving importance to the most recent periods.

At the end of each period i , *BitChop* decides what the mantissa bitlength, n_{i+1} , should be for the next period $i + 1$ as follows:

$$n_{i+1} = \begin{cases} n_i - 1, & \text{when } Mavg_i > L_i + \epsilon \\ n_i, & \text{when } L_i - \epsilon_i \leq Mavg_i \leq L_i + \epsilon_i \\ n_i + 1, & \text{when } Mavg_i < L_i - \epsilon \end{cases} \quad (9)$$

where L_i and n_i are respectively the loss and the mantissa length of period i , and ϵ_i is a threshold calculated with the average relative error between L_i and $Mavg_i$. Full precision is used during LR changes, as the network is more sensitive. *BitChop* is implemented as a simple hardware controller which is notified of the loss via a user-level register in memory. The only modification to the training code is for updating this register once per period.

Evaluation: BitLengths and Accuracy: We measure the effectiveness of *BitChop* by reporting its effect on memory footprint and accuracy during full training sessions of ResNet18 as described for *Quantum Mantissa*. Presently, *BitChop* adjusts the mantissa only for the activations. Figure 6 shows that with *BitChop*, the network achieves the same validation accuracy as with the baseline training. For clarity, the figure shows results for BFloat16 only (results with FP32 were similar and accuracy was unaffected). Throughout the training process, validation accuracy under *BitChop* exhibits more pronounced swings compared to the baseline and to *Quantum Mantissa*. However, in absolute terms, these swings are small as the validation accuracy under *BitChop* closely follows that observed with baseline training.

Figure 7 shows that *BitChop* reduces mantissa bitlengths to 4 - 5 bits on average when used over BFloat16 and to 5 - 6 bits on average when used over FP32. However, the mantissa bitlength may vary per batch depending on the loss. This is illustrated in Figure 8, through a histogram of the bitlengths

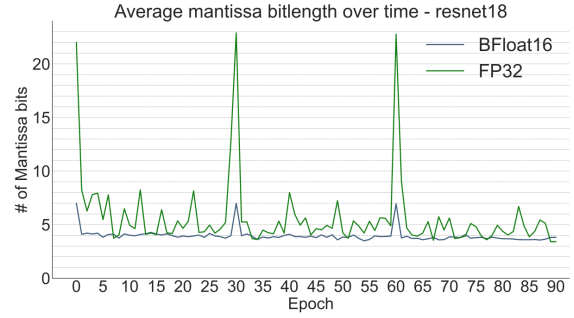


Fig. 7: *BitChop*: ResNet18 average mantissa bitlengths per epoch throughout training, on BFloat16 and FP32.

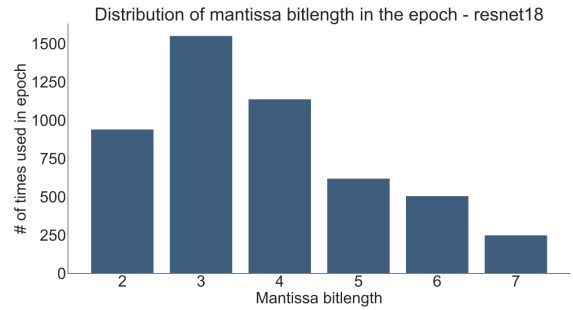


Fig. 8: *BitChop*: ResNet18 - Bfloat16, distribution of *BitChop*'s mantissa bitlengths throughout the 5005 batches of epoch 45 in ImageNet training.

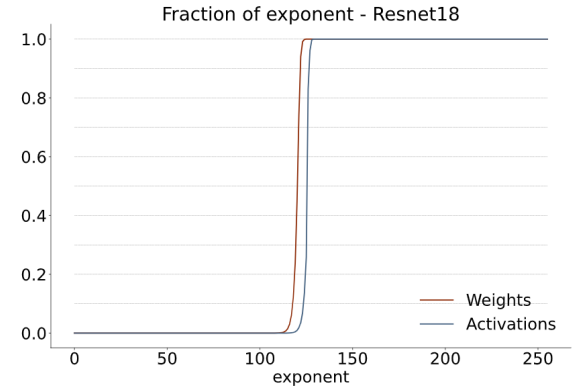


Fig. 9: ResNet18: Distribution of exponent values

used throughout a sample epoch (epoch 45) for the BFloat16 run. This shows that while *BitChop* is consistently reducing the mantissa bitlength to 2 - 4 bits, the training process sometimes requires the entire range of Bfloat16. All across the training process, *BitChop* reduces the total mantissa footprint of the BFloat16 baseline to 64.3%, and over FP32 *BitChop* reduces mantissa footprint to 56.1%.

While *BitChop*'s network-level granularity might miss potential bitlength reductions, the method does not require extra trainable parameters or any modification to the training process.

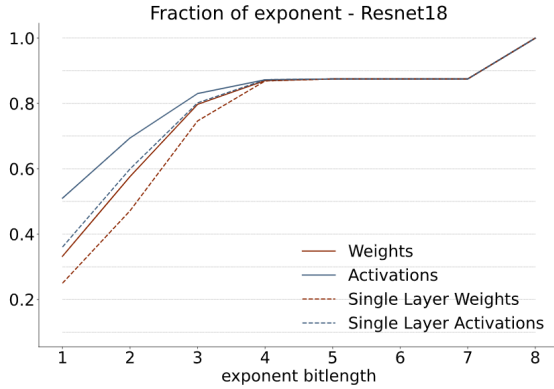


Fig. 10: ResNet18: Post-encoding distribution of exponent bitlength

Nor does it introduce any explicit overhead, making it a plug-in, albeit ad-hoc adjustment to the training process.

C. Exponent: *Gecko*

The exponents of BFloat16 and FP32 are 8b biased fixed-point numbers. Except for a few early batches, we find that during training the exponent values exhibit a heavily biased distribution centered around 127 which represents 0. This is illustrated in Figure 9 which reports the exponent distribution throughout training of Resnet18 after epoch 10 (the figure omits gradients which are even more biased as those can be kept on-chip). Taking advantage of the relatively small magnitude of most exponents we adopt a variable length *lossless* exponent encoding. The encoding uses only as many bits as necessary to represent the specific exponent magnitude rather than using 8b irrespective of value content. Since we use variable-sized exponents, a metadata field specifies the number of bits used. Having a dedicated bitlength per value would negate any benefits or worse become an overhead. To amortize the cost of this metadata several exponents share a common bitlength which is long enough to accommodate the highest magnitude within the group. We further observed that especially for weights, the values often exhibit spatial correlation, that is values that are close-by tend to have similar magnitude. Encoding differences in value skews the distribution closer to zero benefiting our encoding scheme.

In the implementation we study the encoding scheme *Gecko* used is as follows: Given a tensor, *Gecko* first groups the values in groups of 64 (padding as needed) which it treats conceptually as an 8x8 matrix. Every column of 8 exponents is a group which shares a common base exponent. The base exponent per column is the exponent that appears in the first row of incoming data. The base exponent is stored in 8b. The remaining 7 exponents are stored as deltas from the base exponent. The deltas are stored as [magnitude, sign] format and using a bitlength to accommodate the highest magnitude among those per row. A leading 1 detector determines how many bits are needed. The bitlength is stored using 3b and

the remaining exponents are stored using the bitlength chosen. Alternatively, a fixed bias can be used to encode the exponents. In this case, a predetermined bias b is used to encode the exponents in memory where an exponent E is stored as $E - b$ and with as many bits as necessary to store the magnitude of this difference. The bias can be programmed up-front or can be fixed in the design. A bias of 127 was found to be best for the models studied. When this scheme is used, exponents can be encoded in smaller groups. We have found that a group of 8 works very well in practice.

Evaluation: BitLength: We measure how many bits are needed to encode the exponents using *Gecko* and for the duration of training of ResNet18 as described previously. For clarity, we limit attention to BFloat16. As a representative measurement, Figure 10 reports the cumulative distributions of exponent bitlength for one batch across 1) all layers, and 2) for a single layer, and separately for weights and activations. After delta encoding, almost 90% of the exponents become lower than 16. Further, 20% of the weight exponents and 40% of the activation exponents end up being represented using only 1 bit. Across the whole training process, the overall compression ratio for the weight exponents is 0.56 and 0.52 for the activation exponents. The ratio is calculated as $(M + C)/O$ where M the bits used by the per group bitlength fields, C the bits used to encode the exponent magnitudes after compression, and O the bits used to encode exponents in the original format.

D. Sign

One of the simplest and most common activation functions used for CNNs is the Linear Rectifier (ReLU), which zeroes out all negative values. As a result, ReLU outputs can be stored without the sign bit.

V. OUR HARDWARE APPROACH

This section presents the *Schrödinger's FP* hardware encoder/decoder units that efficiently exploit the potential created by our quantization schemes. Without the loss of generality we describe compressors/decompressors that process groups of 64 FP32 values.

A. Compressor

Figure 11a shows that the compressor contains 8 packer units (Figure 11c). The compressor accepts one row (8 numbers) per cycle, for a total of 8 cycles to consume the whole group. Each column is treated as a subgroup whose exponents are to be encoded using the first element's exponent as the base and the rest as deltas. Accordingly, the exponents of the first row are stored as-is via the packers. For the every subsequent row, the compressor first calculates deltas prior to passing them to the packers.

The length of the mantissa is the same for all values and is provided by the mantissa quantizer method be it *Quantum Mantissa* or *BitChop*. Each row uses a container whose bitlength is the sum of the mantissa bitlength (provided externally) plus the bitlength needed to store the highest exponent magnitude cross the row. To avoid wide crossbars when packing/unpacking,

values remain within the confines of their original format bit positions as per the method proposed in Proteus [56]. In contrast to Proteus, however, here every row uses a different bitlength, the values are floating-point, the bitlengths vary during runtime and per row, and we target training. The exponent lengths need to be stored as metadata per row. These are stored separately necessitating two write streams per tensor both however are sequential thus DRAM-friendly. The mantissa lengths are either tensor/layer- or network-wide and are stored along with the other metadata for the model.

Each packer (Figure 11c) takes a single FP32 number in [exponent, sign, mantissa] format, masks out unused exponent and mantissa bits, and rotates the remain bits to position to fill in the output row. The mask is created based on the exp_width and man_width inputs. The rotation counter register provides the rotation count which is updated to $(exp_width + man_width + 1)$ every cycle. The (L,R) register pair, is used to tightly pack the encoded values into successive rows. There are needed since a value may now be split across two memory rows. When either register, its 32b (or 16b for BFloat16) are drained to memory. This arrangement effectively packs the values belonging to this column tightly within a column of 32b in memory. Since each rows the same total bitlength, the 8 packers operate in tandem filling their respective outputs at exactly the same rate. As a result, the compressor produces $8 \times 32b$ at a time. The rate at which the outputs are produced depends on the compression rate achieved, the higher the compression, the lower the rate.

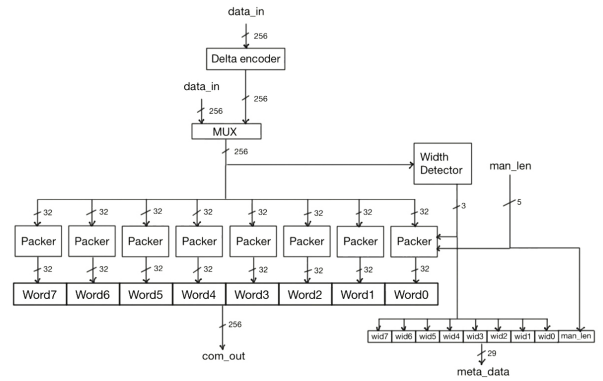
B. Decompressor

As Figure 11b shows, the decompressor mirrors the compressor. It takes 8 3-bit exponent widths and a mantissa length from the system, and 8×32 bits of data per cycle. Every column of 32b is fed into a dedicated unpacker per column. The unpacker (Figure 11d reads the exponent length for this row and the global mantissa length, takes the correct number of bits, and extends the data to [exponent, sign, mantissa] format.

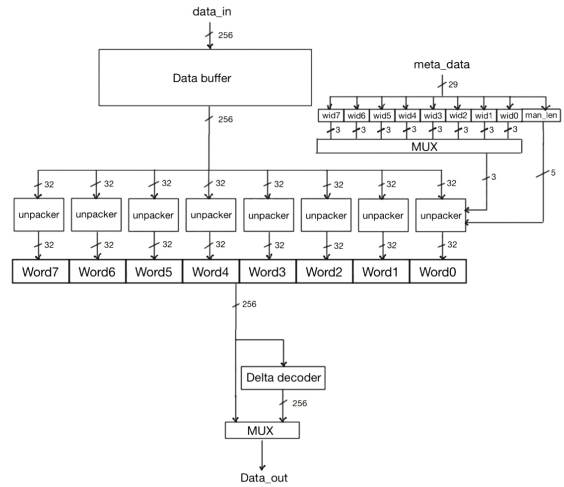
Each unpacker handles one column of 32b from the incoming compressed stream. The combine-and-shift will combine the input data and previous data in register then shift to the left. The number of shifted bits is determined by the exponent and mantissa lengths of this row. The 32-bit data on the left of the register are taken out and shifted to the right (zero extending the exponent). Finally, the unpacker reinserts the mantissa bits that were trimmed during compression. Since each row of data uses the same total bitlength, the unpackers operate in tandem consuming data at the same rate. The net effect is that external memory see wide accesses on both sides.

VI. EVALUATION – PUTTING ALL TOGETHER

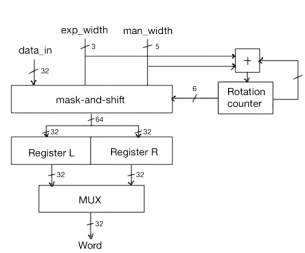
We study the following two *Schrödinger's FP* variants: *Gecko/Quantum Mantissa* (SFP_{QM}) and *Gecko/BitChop* (SFP_{BC}) which are combinations of our exponent and mantissa compression methods and the interaction with GIST++ [24], a slightly modified version of Gist that uses sparsity encoding only for those tensors where doing so reduces footprint avoiding



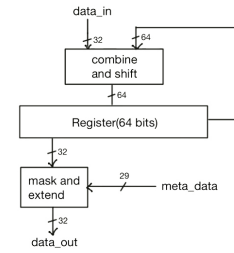
(a) Compressor



(b) Decompressor



(c) Packer



(d) Unpacker

Fig. 11: *Schrödinger's FP* Compressors/Decompressors

the increase in traffic that would occur otherwise. This is especially useful for MobileNet V3 that does not use ReLU.

We perform *full* training runs for ResNet18 [47] and MobileNet V3 Small [48] over ImageNet [49] using an RTX3090/24GB while using PyTorch v1.10. We implement *Quantum Mantissa* by modifying the loss function and adding the gradient calculations for the per tensor/layer parameters. We simulate *BitChop* in software. For both methods, we faithfully emulate mantissa bitlength effects by truncating the mantissa

bits at the boundary of each layer using PyTorch hooks and custom layers. We also implement *Gecko* in software via PyTorch hooks. The above enhancements allow us to measure the effects our methods have on traffic and model accuracy.

A. Memory Footprint Reduction

First we report activation and weight footprint reduction on ResNet18. Combined, our compression techniques excel at reducing memory footprint during training with little affect on accuracy. Table I shows the cumulative total memory reduction in comparison with FP32 and BFloat16 baselines and the corresponding validation accuracies. Our compression methods significantly reduce memory footprint for all tested networks, whilst not significantly affecting accuracy.

1) SFP_{QM} : Figure 12 shows the relative footprint of each part of the datatype with SFP_{QM} in comparison with the FP32 and Bfloat16 baseline. Even though our methods are very effective at reducing the weight footprint (91% for mantissas and 54% for exponents), this effect is negligible in the grand scheme of things due to Amdahl’s law and the fact that weights are a very small part of all three footprints. For the same reason, the reductions in activation footprint (92% for mantissas, 63% for exponents and 98% for sign) have a far greater effect. Because of the effectiveness of *Quantum Mantissa* mantissa compression, the mantissas are reduced from the top contributor in FP32 (70%), to a minor contributor (38%). While exponents are significantly reduced too, they start to dominate with 59% of the footprint in comparison with the FP32 baseline at 24%. Similar conclusions are reached when comparing with Bfloat16 except for the fact that in Bfloat16 mantissas and exponents have similar footprint.

2) SFP_{BC} : Figure 12 also shows the relative footprint of the datatype components under SFP_{BC} when compared to the FP32 and Bfloat16 baselines. While *BitChop* does reduce mantissa bitlength for the network’s weights, this does not have a great effect in the total memory footprint reduction due to the small size of weights when compared to activations. Although mantissa weight footprint is not reduced, weight exponent footprint is by 56%. This is why the focus on the activations’ mantissa bitlengths yields a significant total memory footprint reduction when compared to FP32 (mantissa footprint is reduced by 81%, exponent footprint by 63% and sign by 98% in activations), and a smaller but still significant reduction when compared with Bfloat16 (36% for mantissa and 63% for exponents). The reductions are not as great as with *Quantum Mantissa* due to the network-wise limitation of the method and activation mantissas stay as the major contributor of footprint.

B. Relative compression

Finally we compare *Schrödinger’s FP* compression against Bfloat16, GIST++ and JS, a simple sparse Bfloat16 zero-compression method in Figure 13. JS uses an extra bit per value to avoid storing zeros. We limit attention to activations since we have since that overall weights represent a small fraction of overall footprint and traffic. All methods benefit

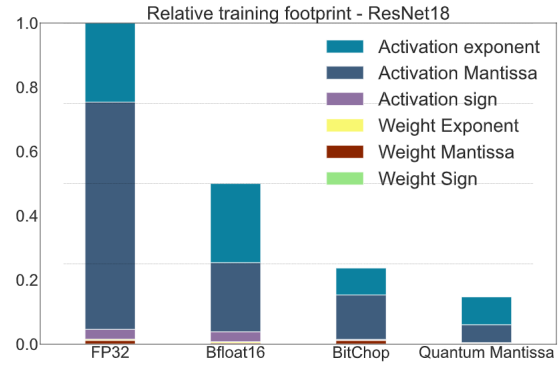


Fig. 12: ResNet18 relative weight and activation footprint: FP32, BF16, SFP_{BC} and SFP_{QM} . ImageNet with batch size 256

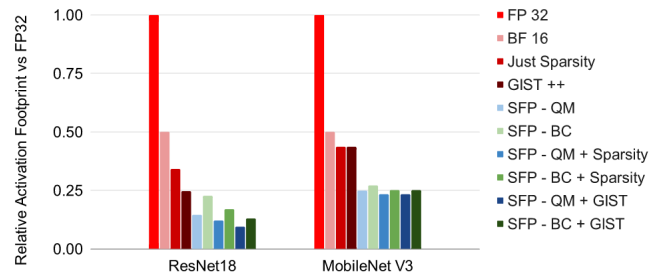


Fig. 13: *Schrödinger’s FP*: Comparison of cumulative activation footprint with BF16, sparsity only and GIST++ compression

from the use of a 16 bit base. On ResNet18, JS and GIST++ benefit from the 30% reduction due to high sparsity induced by ReLu. GIST++ benefits even further because of its efficient compression of maximum pooling. SFP_{BC} does even better just by finding a smaller datatype outperforming all of them, whereas SFP_{QM} proves even better by adjusting the datatype per layer. However, SFP_{BC} and SFP_{QM} only target the reduced datatype and there is opportunity to build on with same ideas that power JS and GIST++. When combined this further improves compression ratios to 10× and 8× for modified SFP_{QM} and SFP_{BC} .

MobileNet V3 small poses a bigger challenge since it sparsely uses ReLu and uses no max pooling. Accordingly, there is little potential for JS and GIST++ to exploit. SFP_{QM} and SFP_{BC} still get another 2× compression over Bfloat16, JS, and GIST++. Application of ideas from JS and GIST++ to *Schrödinger’s FP* compression offers marginal gains.

C. Performance and Energy Efficiency

Since training these networks takes several *days* on actual hardware, cycle-accurate simulation of the full process is impractical. To estimate performance and energy, we analytically model the time and energy used per layer per pass of a baseline accelerator using traffic and compute counts collected during the aforementioned full training runs. We record these counts each time a layer is invoked using PyTorch hooks. We

TABLE I: SFP_{BC} , SFP_{QM} , BF16: Accuracy and total memory reduction vs. FP32.

Network	FP32		BF16	SFP_{QM}		SFP_{BC}	
	Accuracy	Footprint	Footprint	Accuracy	Footprint	Accuracy	Footprint
ResNet18	69.94	100%	50%	69.54	14.7%	69.95	23.7%
MobileNet V3 Small	65.60	100%	50%	65.26	24.9%	65.21	27.2%

TABLE II: Performance and Energy Efficiency gains in comparison with the FP32 baseline. Higher is better

Network	Performance			Energy Efficiency		
	Bfloat 16	SFP_{QM}	SFP_{BC}	Bfloat 16	SFP_{QM}	SFP_{BC}
ResNet18	1.53 \times	2.30 \times	2.15 \times	2.00 \times	6.12 \times	4.54 \times
MobileNet V3 Small	1.72 \times	2.37 \times	2.32 \times	2.00 \times	3.95 \times	3.84 \times

model an accelerator with 8K units each capable of performing 4 MACs per cycle and with a 500MHz clock for a peak computer bandwidth of 16TFLOPS. We consider two baseline accelerators using respectively FP32 and BFloat16. Both have 8 channels of LPDDR4-3200 DRAM memory and 32MB of on-chip buffers. We model time and energy for memory accesses via DRAMSIM3 [57]. For modeling on-chip structures we use CACTI [58] for the buffers and layout measurements for the compute units and the *Gecko* compressors/decompressors. We use a commercial 65nm process to model the processing units and *Gecko* hardware. We implement the units in Verilog and perform synthesis via the Synopsys Design Compiler and layout using Cadence Innovus with a target frequency of 500MHz. Synthesis uses Synopsys’ commercial Building Block IP library for the target tech node. We estimate power via Innovus using traces over a representative sample. There are two *Gecko* compressor/decompressor units per channel.

To take advantage of data reuse where possible we perform the forward pass in a layer-first order per batch. This allows us to read the weights per layer only once per batch. For the backward pass, we utilize the on-chip buffers for mini-batching with a layer-first order over a mini-batch of samples. Mini-batching reduces overall traffic by processing as many samples as possible in a layer-first order avoiding either having to spill gradients or reading and writing weights per sample per layer. The number of samples that can fit in a mini-batch depends on the layer dimensions and the size of the on-chip buffer.

Performance improvements of Bfloat16, SFP_{QM} , and SFP_{BC} over the FP32 baseline are shown in Table II. On average, SFP_{QM} and SFP_{BC} produce a speed up of 2.3 \times and 2.2 \times respectively, while Bfloat 16 speeds up by 1.6 \times . Both SFP_{QM} and SFP_{BC} significantly outperform both the FP32 baseline and the Bfloat 16 on all networks. However, performance does not scale linearly even though SFP_{QM} and SFP_{BC} reduce the memory footprint to 14.7% and 23.7% respectively. This is due to layers that were previously memory bound during the training process now becoming compute bound because of the reduction in memory footprint. This is also the reason why even though Bfloat16 reduces the data type to half, it does not achieve 2 \times speedup. This transition of most layers from memory bound to compute bound also affects the improvements in performance that SFP_{QM} can offer, as even though the method consistently achieves a lower footprint than SFP_{BC} , this only offers an advantage for performance in the few layers that remain memory bound.

SFP_{QM} may offer bigger performance benefits if coupled with higher computational performance hardware that would reduce the computation time of the layers. Regardless, while a reduction in traffic may not yield a direct improvement in performance, it does improve energy efficiency.

Table II also shows the improvement in energy efficiency of Bfloat16, SFP_{QM} and SFP_{BC} over the FP32 baseline. SFP_{QM} and SFP_{BC} excel at improving energy efficiency by significantly reducing DRAM traffic. The energy consumption of DRAM accesses greatly outclasses that of computation, and due to DRAM accesses not being limited by compute bound network layers, SFP_{QM} and SFP_{BC} are more impactful in energy efficiency than in performance improvements, achieving an average of 5.0 \times and 4.1 \times energy efficiency improvements respectively. The dominance of DRAM access energy consumption over computation can also be seen in Bfloat16, where the reduction to half the footprint, the use of 16-bit compute units and the compute layers being no longer a limiting factor gives Bfloat16 a 2 \times energy efficiency improvement.

VII. CONCLUSION

We explored methods that dynamically adapt the bitlengths and containers used for floating-point values during training. The different distributions of the exponents and mantissas led us to tailored approaches for each. In this work we targeted the largest contributors to off-chip traffic during training activations and also the weights. There are several directions for improvements and further exploration including expanding the methods to also target the gradients and refining the underlying policies they use to adapt mantissa lengths. Regardless, this work has demonstrated that the methods are effective. The key advantages of our methods are: 1) they are dynamic and adaptive, 2) they do not modify the training algorithm, 3) they take advantage of value content for the exponents.

ACKNOWLEDGMENTS

This work was supported by a grant from the Samsung Advanced Institute of Technology, the NSERC COHESA Strategic Research Network and an NSERC Discovery Grant. This manuscript was previously submitted to the 2022 International Symposium on Computer Architecture.

REFERENCES

- [1] S. Venkataramani, A. Ranjan, S. Banerjee, D. Das, S. Avancha, A. Jagannathan, A. Durg, D. Nagaraj, B. Kaul, P. Dubey, and A. Raghunathan, "ScaleDeep: A scalable compute architecture for learning and evaluating deep networks," in *Proceedings of the 44th Annual International Symposium on Computer Architecture, ISCA '17*, (New York, NY, USA), pp. 13–26, ACM, 2017.
- [2] D. Amodei, D. Hernandez, G. Sastry, J. Clark, G. Brockman, and I. Sutskever, "Open AI Blog,"
- [3] "NVIDIA Tesla V100 GPU Architecture," in <https://images.nvidia.com/content/volta-architecture/pdf/volta-architecture-whitepaper.pdf>, NVIDIA, 2017.
- [4] N. P. Jouppi, C. Young, N. Patil, D. Patterson, G. Agrawal, R. Bajwa, S. Bates, S. Bhatia, N. Boden, A. Borchers, R. Boyle, P.-I. Cantin, C. Chao, C. Clark, J. Coriell, M. Daley, M. Dau, J. Dean, B. Gelb, T. V. Ghaemmaghami, R. Gottipati, W. Gulland, R. Hagmann, C. R. Ho, D. Hogberg, J. Hu, R. Hundt, D. Hurt, J. Ibarz, A. Jaffey, A. Jaworski, A. Kaplan, H. Khaitan, D. Killebrew, A. Koch, N. Kumar, S. Lacy, J. Laudon, J. Law, D. Le, C. Leary, Z. Liu, K. Lucke, A. Lundin, G. MacKean, A. Maggiore, M. Mahony, K. Miller, R. Nagarajan, R. Narayanaswami, R. Ni, K. Nix, T. Norrie, M. Omernick, N. Penukonda, A. Phelps, J. Ross, M. Ross, A. Salek, E. Samadiani, C. Severn, G. Sizikov, M. Snellman, J. Souter, D. Steinberg, A. Swing, M. Tan, G. Thorson, B. Tian, H. Toma, E. Tuttle, V. Vasudevan, R. Walter, W. Wang, E. Wilcox, and D. H. Yoon, "In-datacenter performance analysis of a tensor processing unit," in *Proceedings of the 44th Annual International Symposium on Computer Architecture, ISCA '17*, (New York, NY, USA), pp. 1–12, ACM, 2017.
- [5] "Gaudi training platform white paper," in <https://habana.ai/wp-content/uploads/2019/06/Habana-Gaudi-Training-Platform-whitepaper.pdf>, Habana, 2019.
- [6] H. Liao, J. Tu, J. Xia, and X. Zhou, "DaVinci: A scalable architecture for neural network computing," in *2019 IEEE Hot Chips 31 Symposium (HCS)*, pp. 1–44, 2019.
- [7] "Cerebras CS1," in <https://www.cerebras.net/product/>, Cerebras, 2019.
- [8] M. Courbariaux, Y. Bengio, and J.-P. David, "Binaryconnect: Training deep neural networks with binary weights during propagations," in *Advances in Neural Information Processing Systems*, pp. 3123–3131, 2015.
- [9] M. Nikolić, M. Mahmoud, and A. Moshovos, "Characterizing sources of ineffectual computations in deep learning networks," in *2018 IEEE International Symposium on Workload Characterization (IISWC)*, pp. 86–87, 2018.
- [10] K. Wang, Z. Liu, Y. Lin, J. Lin, and S. Han, "HAQ: hardware-aware automated quantization," *CoRR*, vol. abs/1811.08886, 2018.
- [11] M. Nikolić, G. B. Hacene, C. Bannon, A. D. Lascorz, M. Courbariaux, Y. Bengio, V. Gripon, and A. Moshovos, "Bitpruning: Learning bitlengths for aggressive and accurate quantization," 2020.
- [12] Y. L. Cun, J. S. Denker, and S. A. Solla, "Optimal brain damage," in *Advances in Neural Information Processing Systems*, pp. 598–605, Morgan Kaufmann, 1990.
- [13] T.-J. Yang, Y.-H. Chen, and V. Sze, "Designing energy-efficient convolutional neural networks using energy-aware pruning," 2017.
- [14] S. Han, H. Mao, and W. J. Dally, "Deep compression: Compressing deep neural network with pruning, trained quantization and Huffman coding," in *4th International Conference on Learning Representations, ICLR 2016, San Juan, Puerto Rico, May 2-4, 2016, Conference Track Proceedings* (Y. Bengio and Y. LeCun, eds.), 2016.
- [15] T. Elsken, J. H. Metzger, and F. Hutter, "Neural architecture search: A survey," *Arxiv preprint arxiv:1808.05377*, 2018.
- [16] J. Snoek, H. Larochelle, and R. P. Adams, "Practical bayesian optimization of machine learning algorithms," in *Proceedings of the 25th International Conference on Neural Information Processing Systems - Volume 2, NIPS'2012*, p. 2951...2959, 2012.
- [17] J. Dean, G. S. Corrado, R. Monga, K. Chen, M. Devin, Q. V. Le, M. Z. Mao, M. Ranzato, A. Senior, P. Tucker, K. Yang, and A. Y. Ng, "Large scale distributed deep networks," in *Proceedings of the 25th International Conference on Neural Information Processing Systems - Volume 1, NIPS'12*, (USA), pp. 1223–1231, Curran Associates Inc., 2012.
- [18] R. Mayer and H. Jacobsen, "Scalable deep learning on distributed infrastructures: Challenges, techniques and tools," *CoRR*, vol. abs/1903.11314, 2019.
- [19] Y.-H. Chen, J. Emer, and V. Sze, "Eyeriss: A spatial architecture for energy-efficient dataflow for convolutional neural networks," in *ACM SIGARCH Computer Architecture News*, vol. 44, pp. 367–379, IEEE Press, 2016.
- [20] W. Wen, C. Xu, F. Yan, C. Wu, Y. Wang, Y. Chen, and H. Li, "TernGrad: Ternary gradients to reduce communication in distributed deep learning," in *Advances in Neural Information Processing Systems 30* (I. Guyon, U. V. Luxburg, S. Bengio, H. Wallach, R. Fergus, S. Vishwanathan, and R. Garnett, eds.), pp. 1509–1519, Curran Associates, Inc., 2017.
- [21] K. Hegde, J. Yu, R. Agrawal, M. Yan, M. Pellauer, and C. W. Fletcher, "UCNN: Exploiting computational reuse in deep neural networks via weight repetition," in *Proceedings of the 45th Annual International Symposium on Computer Architecture, ISCA '18*, (Piscataway, NJ, USA), pp. 674–687, IEEE Press, 2018.
- [22] S. J. Pan and Q. Yang, "A survey on transfer learning," *IEEE Transactions on Knowledge and Data Engineering*, vol. 22, no. 10, pp. 1345–1359, 2010.
- [23] P. Kairouz, H. B. McMahan, B. Avent, A. Bellet, M. Bennis, A. N. Bhagoji, K. A. Bonawitz, Z. Charles, G. Cormode, R. Cummings, R. G. L. D'Oliveira, H. Eichner, S. E. Rouayheb, D. Evans, J. Gardner, Z. Garrett, A. Gascón, B. Ghazi, P. B. Gibbons, M. Gruteser, Z. Harchaoui, C. He, L. He, Z. Huo, B. Hutchinson, J. Hsu, M. Jaggi, T. Javidi, G. Joshi, M. Khodak, J. Konečný, A. Korolova, F. Koushanfar, S. Koyejo, T. Lepoint, Y. Liu, P. Mittal, M. Mohri, R. Nock, A. Özgür, R. Pagh, H. Qi, D. Ramage, R. Raskar, M. Raykova, D. Song, W. Song, S. U. Stich, Z. Sun, A. T. Suresh, F. Tramèr, P. Vepakomma, J. Wang, L. Xiong, Z. Xu, Q. Yang, F. X. Yu, H. Yu, and S. Zhao, "Advances and open problems in federated learning," *Found. Trends Mach. Learn.*, vol. 14, no. 1-2, pp. 1–210, 2021.
- [24] A. Jain, A. Phanishayee, J. Mars, L. Tang, and G. Pekhimenko, "Gist: Efficient data encoding for deep neural network training," in *Proceedings of the 45th Annual International Symposium on Computer Architecture, ISCA '18*, (Piscataway, NJ, USA), pp. 776–789, IEEE Press, 2018.
- [25] T. Chen, B. Xu, C. Zhang, and C. Guestrin, "Training deep nets with sublinear memory cost," *CoRR*, vol. abs/1604.06174, 2016.
- [26] Y. Huang, Y. Cheng, D. Chen, H. Lee, J. Ngiam, Q. V. Le, and Z. Chen, "Gpipe: Efficient training of giant neural networks using pipeline parallelism," *CoRR*, vol. abs/1811.06965, 2018.
- [27] S. Wang and P. Kanwar, "BFloat16: The secret to high performance on cloud TPUs," in <https://cloud.google.com/blog/products/ai-machine-learning/bfloat16-the-secret-to-high-performance-on-cloud-tpus>, Google, 2019.
- [28] D. D. Kalamkar, D. Mudigere, N. Mellempudi, D. Das, K. Banerjee, S. Avancha, D. T. Vooturi, N. Jammalamadaka, J. Huang, H. Yuen, J. Yang, J. Park, A. Heinecke, E. Georganas, S. Srinivasan, A. Kundu, M. Smelyanskiy, B. Kaul, and P. Dubey, "A study of BFloat16 for deep learning training," *CoRR*, vol. abs/1905.12322, 2019.
- [29] Google, "Using bfloat16 with tensorflow models." <https://cloud.google.com/tpu/docs/bfloat16>.
- [30] D. Das, N. Mellempudi, D. Mudigere, D. D. Kalamkar, S. Avancha, K. Banerjee, S. Sridharan, K. Vaidyanathan, B. Kaul, E. Georganas, A. Heinecke, P. Dubey, J. Corbal, N. Shustrov, R. Dubtsov, E. Fomenko, and V. O. Pirogov, "Mixed precision training of convolutional neural networks using integer operations," in *6th International Conference on Learning Representations, ICLR 2018, Vancouver, BC, Canada, April 30 - May 3, 2018, Conference Track Proceedings*, 2018.
- [31] U. Köster, T. J. Webb, X. Wang, M. Nassar, A. K. Bansal, W. H. Constable, O. H. Elibol, S. Gray, S. Hall, L. Hornof, A. Khosrowshahi, C. Kloss, R. J. Pai, and N. Rao, "Flexpoint: An adaptive numerical format for efficient training of deep neural networks," in *Proceedings of the 31st International Conference on Neural Information Processing Systems, NIPS'17*, (USA), pp. 1740–1750, Curran Associates Inc., 2017.
- [32] P. Micikevicius, S. Narang, J. Alben, G. F. Diamos, E. Elsen, D. Garcia, B. Ginsburg, M. Houston, O. Kuchaiev, G. Venkatesh, and H. Wu, "Mixed precision training," in *6th International Conference on Learning Representations, ICLR 2018, Vancouver, BC, Canada, April 30 - May 3, 2018, Conference Track Proceedings*, 2018.
- [33] NVIDIA, "Training with mixed precision." <https://docs.nvidia.com/deeplearning/sdk/mixed-precision-training/index.html>.
- [34] M. Drummond, T. Lin, M. Jaggi, and B. Falsafi, "Training DNNs with hybrid block floating point," in *Proceedings of the 32nd International Conference on Neural Information Processing Systems, NIPS'18*, (USA), pp. 451–461, Curran Associates Inc., 2018.

- [35] C. De Sa, M. Leszczynski, J. Zhang, A. Marzoev, C. R. Aberger, K. Olukotun, and C. Ré, “High-accuracy low-precision training,” *arXiv preprint arXiv:1803.03383*, 2018.
- [36] M. Rhu, M. O’Connor, N. Chatterjee, J. Pool, Y. Kwon, and S. W. Keckler, “Compressing dma engine: Leveraging activation sparsity for training deep neural networks,” in *2018 IEEE International Symposium on High Performance Computer Architecture (HPCA)*, pp. 78–91, 2018.
- [37] B. Zheng, N. Vijaykumar, and G. Pekhimenko, “Echo: Compiler-based GPU memory footprint reduction for LSTM RNN training,” in *Proceedings of the 47th Annual International Symposium on Computer Architecture*, ISCA ’20, ACM, 2020.
- [38] R. D. Evans, L. F. Liu, and T. Aamodt, “JPEG-ACT: A frequency-domain lossy DMA engine for training convolutional neural networks,” in *Proceedings of the 47th Annual International Symposium on Computer Architecture*, ISCA ’20, ACM, 2020.
- [39] S. Han, H. Mao, and W. J. Dally, “Deep Compression: Compressing Deep Neural Networks with Pruning, Trained Quantization and Huffman Coding,” *arXiv:1510.00149 [cs]*, Oct. 2015. arXiv: 1510.00149.
- [40] Chen, Yu-Hsin and Krishna, Tushar and Emer, Joel and Sze, Vivienne, “Eyeriss: An Energy-Efficient Reconfigurable Accelerator for Deep Convolutional Neural Networks,” in *IEEE International Solid-State Circuits Conference, ISSCC 2016, Digest of Technical Papers*, pp. 262–263, 2016.
- [41] S. Han, X. Liu, H. Mao, J. Pu, A. Pedram, M. A. Horowitz, and W. J. Dally, “EIE: efficient inference engine on compressed deep neural network,” in *43rd ACM/IEEE Annual International Symposium on Computer Architecture, ISCA 2016, Seoul, South Korea, June 18-22, 2016*, pp. 243–254, 2016.
- [42] S. Liu, Z. Du, J. Tao, D. Han, T. Luo, Y. Xie, Y. Chen, and T. Chen, “Cambricon: An instruction set architecture for neural networks,” *2016 ACM/IEEE 43rd Annual International Symposium on Computer Architecture (ISCA)*, vol. 00, no. undefined, pp. 393–405, 2016.
- [43] A. D. Lascorz, S. Sharify, I. Edo, D. M. Stuart, O. M. Awad, P. Judd, M. Mahmoud, M. Nikolić, K. Siu, Z. Poulos, and A. Moshovos, “Shapeshifter: Enabling fine-grain data width adaptation in deep learning,” in *Proceedings of the 52nd Annual IEEE/ACM International Symposium on Microarchitecture, MICRO 52*, (New York, NY, USA), Association for Computing Machinery, 2019.
- [44] I. Edo Vivancos, S. Sharify, D. Ly-Ma, A. Abdelhadi, C. Bannon, M. Nikolić, M. Mahmoud, A. Delmas Lascorz, G. Pekhimenko, and A. Moshovos, “Boveda: Building an on-chip deep learning memory hierarchy brick by brick,” in *Proceedings of Machine Learning and Systems* (A. Smola, A. Dimakis, and I. Stoica, eds.), vol. 3, pp. 1–20, 2021.
- [45] J. Albericio, P. Judd, T. Hetherington, T. Aamodt, N. Enright Jerger, and A. Moshovos, “Cnvlutin: Ineffectual-Neuron-Free Deep Neural Network Computing,” in *Intl’ Symp. on Computer Architecture*, 2016.
- [46] O. M. Awad, M. Mahmoud, I. Edo, A. H. Zadeh, C. Bannon, A. Jayarajan, G. Pekhimenko, and A. Moshovos, “Fpraker: A processing element for accelerating neural network training,” in *MICRO ’21: 54th Annual IEEE/ACM International Symposium on Microarchitecture, Virtual Event, Greece, October 18-22, 2021*, pp. 857–869, ACM, 2021.
- [47] K. He, X. Zhang, S. Ren, and J. Sun, “Deep residual learning for image recognition,” *CoRR*, vol. abs/1512.03385, 2015.
- [48] A. Howard, M. Sandler, G. Chu, L. Chen, B. Chen, M. Tan, W. Wang, Y. Zhu, R. Pang, V. Vasudevan, Q. V. Le, and H. Adam, “Searching for mobilenetv3,” *CoRR*, vol. abs/1905.02244, 2019.
- [49] O. Russakovsky, J. Deng, H. Su, J. Krause, S. Satheesh, S. Ma, Z. Huang, A. Karpathy, A. Khosla, M. Bernstein, A. C. Berg, and L. Fei-Fei, “ImageNet Large Scale Visual Recognition Challenge,” *arXiv:1409.0575 [cs]*, Sept. 2014. arXiv: 1409.0575.
- [50] X. Sun, N. Wang, C.-Y. Chen, J. Ni, A. Agrawal, X. Cui, S. Venkataramani, K. El Maghraoui, V. V. Srinivasan, and K. Gopalakrishnan, “Ultra-low precision 4-bit training of deep neural networks,” in *Advances in Neural Information Processing Systems* (H. Larochelle, M. Ranzato, R. Hadsell, M. F. Balcan, and H. Lin, eds.), vol. 33, pp. 1796–1807, Curran Associates, Inc., 2020.
- [51] C. Sakr, N. Wang, C.-Y. Chen, J. Choi, A. Agrawal, N. R. Shanbhag, and K. Gopalakrishnan, “Accumulation bit-width scaling for ultra-low precision training of deep networks,” in *7th International Conference on Learning Representations, ICLR 2019, New Orleans, LA, USA, May 6-9, 2019*, OpenReview.net, 2019.
- [52] Y. LeCun, Y. Bengio, and G. Hinton, “Deep learning,” *Nature*, vol. 521, pp. 436–444, 05 2015.
- [53] Y. Bengio, N. Léonard, and A. Courville, “Estimating or propagating gradients through stochastic neurons for conditional computation,” *arXiv preprint arXiv:1308.3432*, 2013.
- [54] I. Hubara, M. Courbariaux, D. Soudry, R. El-Yaniv, and Y. Bengio, “Binarized neural networks,” in *Advances in neural information processing systems*, pp. 4107–4115, 2016.
- [55] K. He, X. Zhang, S. Ren, and J. Sun, “Deep residual learning for image recognition,” in *Proceedings of the IEEE conference on computer vision and pattern recognition*, pp. 770–778, 2016.
- [56] P. Judd, J. Albericio, T. Hetherington, T. M. Aamodt, N. E. Jerger, and A. Moshovos, “Proteus: Exploiting numerical precision variability in deep neural networks,” in *Proceedings of the 2016 International Conference on Supercomputing, ICS ’16*, (New York, NY, USA), pp. 23:1–23:12, ACM, 2016.
- [57] S. Li, Z. Yang, D. Reddy, A. Srivastava, and B. Jacob, “Dramsim3: A cycle-accurate, thermal-capable dram simulator,” *IEEE Computer Architecture Letters*, vol. 19, no. 2, pp. 106–109, 2020.
- [58] HewlettPackard, “CACTI.” <https://github.com/HewlettPackard/cacti>.